Dedicated to Academician Aureliu Sandulescu's 80^{th} Anniversary

APPLICATIONS OF A SEMI-MICROSCOPIC CLUSTER MODEL FOR ASTROPHYSICAL PROCESSES

H. YÉPEZ-MARTÍNEZ[1], P. R. FRASER[2,a], P. O. HESS[2,b]

[1]Universidad Autónoma de la Ciudad de México,
Prolongación San Isidro 151, Col. San Lorenzo Tezonco, Del. Iztapalapa, 09790 México D.F., Mexico
Email: huitzilin_yepez@yahoo.com.mx
[2]Instituto de Ciencias Nucleares, Universidad Nacional Autónoma de México,
Circuito Exterior, C.U., 04510 México, D.F., Mexico
Email: [a]paul.fraser@nucleares.unam.mx, [b]hess@nucleares.unam.mx

Received September 7, 2011

The *Semimicroscopic Algebraic Cluster Model* (SACM) is applied to the two-cluster systems ^{14}C+α and ^{20}Ne+α, which are of astrophysical interest. The parameters of this algebraic model are adjusted to experimental data, being eigenenergies and $B(E2)$ values. After that, sole $B(M1)$ values and α-spectroscopic factors are calculated. The last represent a prediction of this model. Also the geometrical mapping of the SACM is shortly reviewed. The geometric potential, as a function of the coherent state parameter α is constructed. The minimum of the potential shows the position of the systems in the phase space diagram.

1. INTRODUCTION

In [1–4] it was shown that the Pauli exclusion principle has a dramatic effect when combining nucleons of two separate clusters into a composite nucleus which does not behave as a nuclear molecule. Two cluster models were considered that use the same Hamiltonian: a Phenomenological Algebraic Cluster Model (PACM), and a Semimicroscopic Algebraic Cluster Model (SACM) [5, 6]. Both use a modified version of the vibron model [7] to describe relative motion, and the $SU(3)$ model of Elliott [8] for internal cluster structure. The true vibron model describes clusters with the IBA [9, 10], and treats $\hbar\omega$ as a parameter, where here it is fixed by shell model considerations. The difference between PACM and SACM is that the latter includes the Pauli exclusion principle for the combination of the nucleons of the two clusters.

It was shown that this inclusion of the Pauli principle dramatically changed the phase space of the nuclear potential. The inclusion is performed by restricting the nuclear Hilbert space to include only states also present in shell model calculations which includes as an ingredient a minimal number of quanta to the composite system as prescribed by the Wildermuth condition [11], It was also found that with the PACM, nuclear spectra could not be realistically recreated.

In this paper, a resumé of the SACM formalism is presented, followed by two examples of optimal fits to spectral and electromagnetic transition data of nuclei of

astrophysical significance. Energy spectra, $B(E2)$, $B(M1)$ and α-spectroscopic factors will be calculated. Especially the spectroscopic factors can be of interest in astrophysics where nuclei plus α clusters are considered [12]. Two systems, where one cluster is the α particle, are considered, namely ^{14}C+α and ^{20}Ne+α. These are important astrophysical systems for the understanding of element productions in stars, where in the stellar interior a large amount of He-particles are still present. We also considered in recent publications two spherical clusters (^{16}O+α) [1,2]. Their spectral properties and spectroscopic factors are particular simple and will, therefore, neither be considered here, nor the calculations will be repeated. In [13] the ^{14}C+α system has also been discussed within the SACM. The spectrum, E2- and E1-transitions were calculated but no M1-transitions and spectroscopic factors. The Hamiltonian used is different, *e.g.* the quadrupole-quadrupole interaction is repulsive.

It should be noted that here we use the *weak* definition of clusterization, *i.e.* that an overlap of the wave function of the united nucleus has an overlap with a given clusterization. For example, ^{16}O has an overlap with the clusterization ^{12}C+α, though ^{12}C is highly deformed while ^{16}O is spherical. The reason for this is the antisymmetrization of all nucleons which finally produces a spherical united cluster. We will not deal with the *strong* definition of clusterization, which requires the physical separation of the two clusters, as in the $\alpha + \alpha \rightarrow ^{8}$Be system. Even in the weak definition, not all states have an overlap with a certain clusterization. Experimentally, an overlap is given when in a nuclear dispersion, given by two clusters in the incoming channel, states of the united nucleus are occupied.

This contribution is in honor of Prof. Dr. A. Sandulescu, a friend whom P. O. Hess has appreciated greatly since the 1970s. One of his main contribution to physics is on the topic of nuclear cluster physics, especially in cluster radioactivity, predicted by him and his colleagues [14]. Therefore, our contribution on an algebraic nuclear cluster model fits perfectly well in this volume.

The paper is organized as follows: In section II the *Semimicroscopic Algebraic Cluster Model* (SACM) [5, 6] is shortly reviewed. The investigation presented relies heavily on that model. In section III two systems, relevant in astrophysics, are treated within this model. Energies and $B(E2)$ values are fitted, while finally we present the numerical results of the spectrum, $B(E2)$, $B(M1)$ values and α-spectroscopic factors. In section IV the geometrical mapping of the algebraic Hamiltonian is shortly reviewed and the potentials of the two systems are calculated. In section V conclusions are drawn.

2. FORMALISM

2.1. THE MODEL SPACE AND THE HAMILTONIAN

In this model, the relative motion degrees of freedom between the clusters are oscillators in 3 dimensions, plus an additional auxiliary scalar boson, described by boson creation and annihilation operators:

$$\boldsymbol{\pi}^{\dagger}_{m},\, \boldsymbol{\pi}_{m},\, m=\pm 1 \quad ;\, \sigma^{\dagger}, \sigma, \tag{1}$$

where the σ-bosons have no physical interpretation, but define a cut-off for a conserved total number of bosons,

$$N = n_{\pi} + n_{\sigma}. \tag{2}$$

Note, in other formalisms N is the total number of particles. Here it is the total number of bosons of excitation.

We consider 2 clusters, and thus the group structure is [5, 6]

$$\begin{array}{ccccccc} SU_{C_1}(3) \otimes SU_{C_2}(3) \otimes SU_R(3) & \supset & SU_C(3) \otimes SU_R(3) & \supset \\ (\lambda_1,\mu_1) \quad (\lambda_2,\mu_2) \quad (n_{\pi},0) & & (\lambda_C,\mu_C) \\ SU(3) & \supset & SO(3) & \supset & SO(2) \\ (\lambda,\mu) & & \kappa L & & M\,. \end{array} \tag{3}$$

(λ_k, μ_k) refer to the $SU_{C_k}(3)$ irreducible representations (irrep) of individual clusters, which are coupled to intermediate irrep (λ_C, μ_C), those of the Elliott model [8]. R refers to relative motion. Multiplicity indices, not shown here, are defined in [5,6].

The Hamiltonian is given in terms of Casimir operators of the possible subgroups of $SU_{C_1}(3) \otimes SU_{C_2}(3) \otimes SU_R(3)$, allowing for the study of dynamical symmetries. For example, the algebraic quadrupole generators of $SU(3)$, $\boldsymbol{Q}^{a}_{22}$, has a relative term plus a term for each cluster, giving $\boldsymbol{\mathcal{C}}_2(n_{\pi},0) + \boldsymbol{\mathcal{C}}_2(\lambda_C,\mu_C) +$ a relative interaction term. Thus this is a different approach to having a Hamiltonian of the form $\boldsymbol{H}_{C_1} + \boldsymbol{H}_{C_2} + \boldsymbol{H}_{rel.}$. Note also, we use the notation $\boldsymbol{L}^2$ for $(\boldsymbol{L}_R + \boldsymbol{L}_{C_1} + \boldsymbol{L}_{C_2})^2$, subsuming the expansion of which (*i.e.* clusters terms, plus relative motion term, plus interaction terms) into one term. The Hamiltonian can be expressed as

$$\boldsymbol{H} = xy\boldsymbol{H}_{SU(3)} + y(1-x)\boldsymbol{H}_{SO(4)} + (1-y)\boldsymbol{H}_{SO(3)}, \tag{4}$$

which interpolates between the strong coupling limit, $SU(3)$ ($x = y = 1$), the deformed limit, $SO(4)$ ($x = 0$ and $y = 1$), and the weak coupling limit, $SO(3)$ (x arbitrary and $y = 0$) (according to the classification given in [15]). x and y are between 0 and 1, with $y = 0$ defining the $SO(3)$ limit, $x = 0$ and $y = 1$ the $SO(4)$ limit, and $x = y = 1$ the $SU(3)$ limit. (An investigation of moving between two of these limits can be found in [16], and between all three in [2,3].) The notation of the three

limits is as follows: When $x = 1$ and $y = 1$ the strong quadrupole interaction and other $SU(3)$ interaction appear, then we denote it as a *strong limit*. For $x = 0$ and $y = 1$ only $SO(4)$ interactions appear, which always produces a deformed potential, hence the notation of a *deformed limit*. When $y = 0$ then only $\hbar\omega \boldsymbol{n}_\pi$ and terms in the angular momentum operators $\boldsymbol{L}^2$, $\boldsymbol{L}_C^2$ and $\boldsymbol{L}_R$ appear, *i.e.* only angular momenta interactions appear, hence the notation of a *weak coupling limit*.

The components of this Hamiltonian are

$$\hat{H}_{SU(3)} = \hbar\omega \boldsymbol{n}_\pi + a_C \boldsymbol{\mathcal{C}}_2(\lambda_C, \mu_C) + (a - b\Delta \boldsymbol{n}_\pi)\boldsymbol{\mathcal{C}}_2(\lambda, \mu) + (\bar{a} - \bar{b}\Delta \boldsymbol{n}_\pi)\boldsymbol{\mathcal{C}}_2(n_\pi, 0) + \gamma \boldsymbol{L}^2 + t\boldsymbol{K}^2, \quad (5)$$

$$\hat{H}_{SO(4)} = a_C \boldsymbol{L}_C^2 + a_R^{(1)} \boldsymbol{L}_R^2 + \gamma \boldsymbol{L}^2 + \frac{c}{4}\left[\left(\boldsymbol{\pi}^\dagger \cdot \boldsymbol{\pi}^\dagger\right) - \left(\boldsymbol{\sigma}^\dagger\right)^2\right]\left[(\boldsymbol{\pi}\cdot\boldsymbol{\pi}) - (\boldsymbol{\sigma})^2\right] \quad (6)$$

and

$$\hat{H}_{SO(3)} = \hbar\omega \boldsymbol{n}_\pi + a_C \boldsymbol{L}_C{}^2 + a_R^{(1)} \boldsymbol{L}_R{}^2 + \gamma \boldsymbol{L}^2, \quad (7)$$

where C denotes 'cluster' – see (3), R is again 'relative', and $\boldsymbol{K}$ is the angular momentum projection operator onto a fixed-body axis. This term is zero when considering two spherical clusters.

The $\boldsymbol{K}^2$ operator is defined in [5, 6], to describe states in the united nucleus of the same (λ, μ) and L belonging to different bands. It is of microscopic origin (see [17]).

The term $\triangle \boldsymbol{n}_\pi = \boldsymbol{n}_\pi - n_0$ gives rise to cubic terms in resultant potentials. Without it the Hamiltonian would have the proportionality $H \sim \boldsymbol{n}_\pi - \boldsymbol{n}_\pi^2$, with the $\hat{n}_\pi$ latter dominating at high n_π. This pulls states with many quanta of excitation to lower energies than those of few. One method of overcoming this is to restrict to low N, but this avoids, rather than solves, the problem. For details see [17] and references therein. (That work involves a different model, but the same problem applies.)

Normally, in algebraic models a dynamic symmetry limit provides analytic solutions for the energy spectrum. Here, this is the case for the $SU(3)$ limit. However, this is not the case for the $SO(4)$ dynamical symmetry limit, though only the pairing Casimir operator and Casimir operators of subgroups of $SO(4)$ appear. The reason is the implementation of the Pauli exclusion principle, best done within the $SU(3)$ basis. When a $SO(4)$ state is expanded in this basis, basis states appear with a number of relative oscillation quanta less than n_0, thus violating the Pauli exclusion principle. Implementing it requires cutting these components from the $SO(4)$ states. Therefore, the $SO(4)$ symmetry is broken, though, we still will denote it as a dynamical symmetry.

3. RESULTS

First, we will adjust each system to experimental data, being several states of the spectrum and $B(E2)$ values. Second, we list the results for the $B(E2)$ and $B(M1)$ values. In subsection C, the transition operators will be defined. Third, the spectroscopic factors, according to the theory, will be determined and listed.

3.1. THE SYSTEM ^{14}C+$\alpha \rightarrow {}^{18}$O

^{18}O, important in astrophysics, is investigated here as an overlap of the basis states of the clusters ^{14}C+α. The minimal number or quanta, n_0, required to satisfy the Wildermuth condition for combining these two clusters is 6. This is illustrated by Fig. 1.

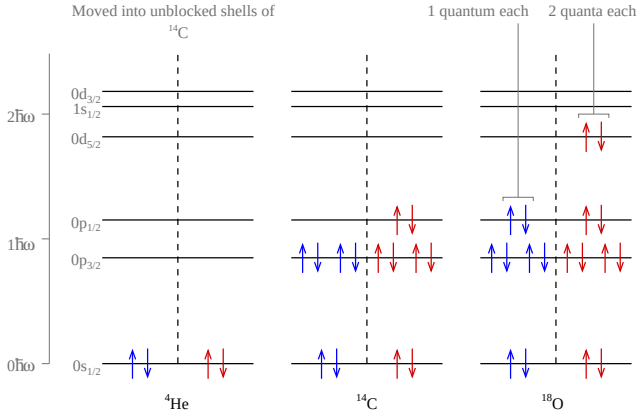

Fig. 1 – This figure illustrates that in order to combine an α-particle with ^{14}C to create ^{18}O, a minimum of 6 quanta of energy are needed to promote the nucleons into unoccupied subshells. This is the Wildermuth condition [11].

Firstly, the shell model space to which the cluster model space is matched was calculated, using numerical routine which can be delivered on request. In the cases of there being n_0 to $n_0 + 9$ quanta of excitation in the composite nucleus, the shell space considered consists of all configurations of the 18 nucleons in the zeroth to fifth shells, where only one of the zeroth and first shells, closed in the ground state, have been opened, and where there are three or less open shells of valence particles. For the cases of there being $n_0 + 10$ and $n_0 + 11$ quanta, only 20 of the possible configurations matching the above criteria were chosen. This leads to the shell model Hilbert space listed in Table 1, which was found to be sufficiently large to describe the system.

The spectral data to which the parameters of the Hamiltonian were matched are shown in Table 2. The eigenstates are those appropriate to this cluster system as

Table 1.

Shell space of ^{14}C+α.

n_0+N	λ_1	μ_1	λ_2	μ_2	λ	μ
6	0	0	0	2	4	0
7	0	0	0	2	5	0
7	0	0	0	2	6	1
8	0	0	0	2	6	0
8	0	0	0	2	8	2
9	0	0	0	2	7	0
9	0	0	0	2	8	1
9	0	0	0	2	9	2
10	0	0	0	2	8	0
10	0	0	0	2	9	1
10	0	0	0	2	10	2
11	0	0	0	2	9	0
11	0	0	0	2	10	1
11	0	0	0	2	11	2
12	0	0	0	2	10	0
12	0	0	0	2	11	1
12	0	0	0	2	12	2
13	0	0	0	2	11	0
13	0	0	0	2	12	1
13	0	0	0	2	13	2
14	0	0	0	2	12	0
14	0	0	0	2	13	1
14	0	0	0	2	14	2
15	0	0	0	2	13	0
15	0	0	0	2	14	1
15	0	0	0	2	15	2
16	0	0	0	2	14	0
16	0	0	0	2	15	1
16	0	0	0	2	16	2
17	0	0	0	2	15	0
17	0	0	0	2	16	1
17	0	0	0	2	17	2

listed in [18], and the $B(E2)$ values are from the studies of [19]. The agreement to experiment is quite good.

These spectral results are presented also in Fig. 2. Therein, solid lines represent states in the ^{18}O nucleus for which $^{14}\mathrm{C}(\alpha,\gamma)$ is a populating reaction. On the experimental side, thin solid lines are unfitted $^{14}\mathrm{C}(\alpha,\gamma)$ states, and *dashed lines represent states which are not populated by this reaction*. On the fit side, long dashed lines represent states predicted by the calculation that do not correspond to fitted data. Note that not all state in the model appear in experiment and call for more measurements.

The optimal parameters of the model which created this match to data are listed in Table 3.

Table 2.

^{14}C+α spectrum data: state spin-parity, experimental energy, and fit energy; followed by $B(E2)$ data: initial state spin-parity, final state spin-parity, experimental transition value, and fit transition value.

J^π	$E_{exp.}$ (MeV)	E_{fit} (MeV)
0_1^+	0.000	0.000
0_2^+	3.633	3.592
2_1^+	1.982	1.173
2_2^+	3.920	4.730
4_1^+	3.554	3.910
4_2^+	7.117	7.466
1_1^-	4.455	3.407
3_1^-	5.097	5.362
5_1^-	7.864	8.881

J_i^π	J_f^π	$B(E2)_{exp.}$ (W.u.)	$B(E2)_{fit}$ (W.u.)
2_1^+	0_1^+	3.32	3.74
4_2^+	2_2^+	3.2	1.83

The best fit for ^{18}O is obtained with the symmetry mixing parameter values $x = y = 1$, *i.e.*, the model interprets this system as being pure $SU(3)$. The positive and negative parity eigenstates are matched well to data, as are the two chosen $B(E2)$ values. The theoretical energies for the first five positive-parity states for each spin are listed in Table 10, and the first five negative-parity states for each spin are listed in Table 11. These tables are found in Section 3.4.

3.2. THE SYSTEM ^{20}Ne+$\alpha \rightarrow {}^{24}$Mg

The ^{24}Mg nucleus is investigated as an overlap of the basis states of the clusters ^{20}Ne+α. The minimal number of quanta, n_0, required to satisfy the Wildermuth condition for combining these two clusters is 8.

Firstly, the shell model space to which the cluster model space is matched was calculated. In the cases of there being n_0 to $n_0 + 9$ quanta of excitation in the composite nucleus, the shell space considered consists of all configurations of the 24 nucleons in the zeroth to fifth shells, where only one of the zeroth and first shells, closed in the ground state, have been opened, and where there are three or less open shells of valence particles. For the cases of there being $n_0 + 10$, $n_0 + 11$, and $n_0 + 12$ quanta, only 20 of the possible configurations matching the above criteria were chosen. This leads to the shell model Hilbert space listed in Table 4. This table lists only the states up to $N + n_0 = 14$. Listing all states would cover more than one page. The full content can be delivered on request.

The spectral data to which the parameters of the Hamiltonian were matched

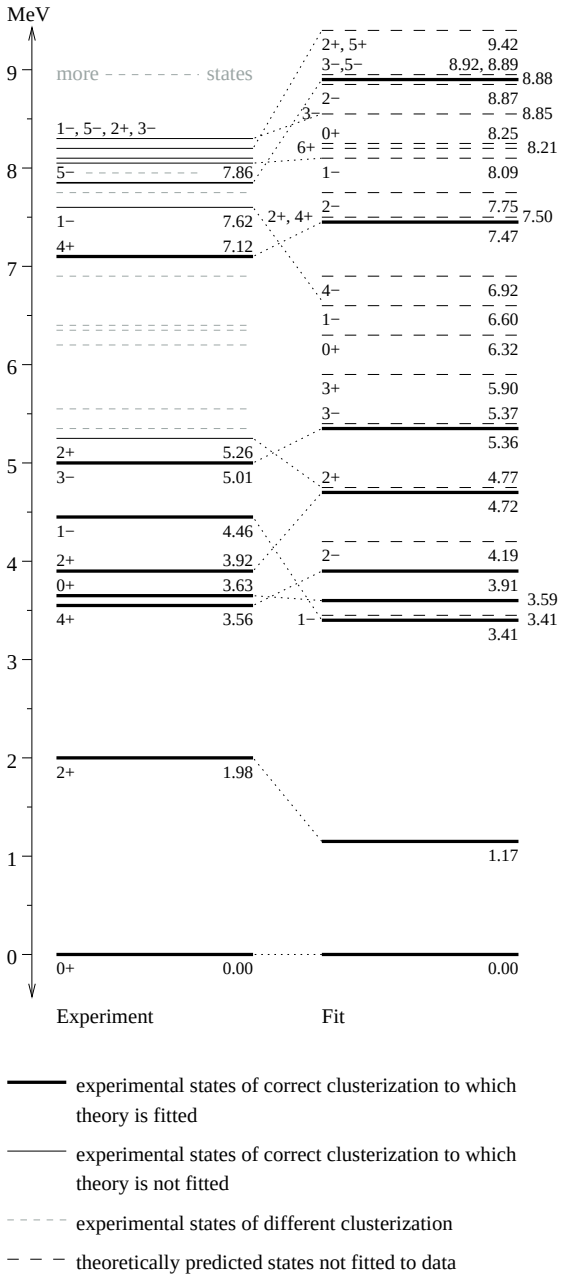

Fig. 2 – The experimental ^{18}O spectrum, and that calculated from SACM evaluation of the ^{14}C+α system.

are shown in Table 5. The eigenstates are those appropriate to this cluster system as listed in [20], and also the $B(E2)$ values are taken from there.

These spectral results are presented also in Fig. 3. Therein, solid lines represent states which were fitted to the model, while the dashed lines represent unfitted states.

The optimal parameters of the model which created this match to data are listed in Table 6.

The best fit for ^{24}Mg is obtained with the mixing parameter values $x = y = 1$, *i.e.* the SACM interprets this system as pure $SU(3)$. The positive and negative parity eigenstates are matched well to data, as are the two chosen $B(E2)$ transitions. The theoretical energies for the first five positive-parity states for each spin are listed in Table 12, and the first five negative-parity states for each spin are listed in Table 13. These tables are found in Section 3.4.

3.3. $B(E2)$ AND $B(M1)$ VALUES

In this section, we list some $B(E2)$ and $B(M1)$ values for the systems ^{14}C+α and ^{20}Ne+α. The transition operators within the model are defined as [6]

$$\boldsymbol{T}^{(E2)}_m = \sum_\gamma e^{(2)}_\gamma \boldsymbol{Q}^{(2)}_{\gamma,m}, \qquad \boldsymbol{T}^{(M1)}_m = \sum_\gamma m^{(1)}_\gamma \boldsymbol{L}^{(1)}_{\gamma,m}. \tag{8}$$

Table 3.

Parameter values defining the ^{14}C+α interaction. The p_{e2} parameter is the effective charge of the charged quadrupole operator, as defined in subsection C.

Hamiltonian and transition							
a	$\bar{a}$	γ	a_{Clus}	$\bar{b}$	b		
-0.202	-0.636	0.195	0.0	-0.005	-0.032		
c	a_C	$a^{(1)}_R$	t	p_{e2}			
0.0	0.0	0.0	0.889	0.334			
Symmetry mixing							
		x	y				
		1.0	1.0				
Clusters							
λ_1	μ_1	$N_{0,1}$	β_1	λ_2	μ_2	$N_{0,2}$	β_2
0	0	4.5	0.00	0	2	29.5	0.32
Quanta							
		$\hbar\omega$	n_0	N			
		13.53	6	11			

Table 4.

Shell space of ^{20}Ne+α.

n_0+N	λ_1	μ_1	λ_2	μ_2	λ	μ
8	0	0	8	0	0	8
8	0	0	8	0	4	6
8	0	0	8	0	8	4
9	0	0	8	0	1	8
9	0	0	8	0	3	7
9	0	0	8	0	5	6
9	0	0	8	0	7	5
9	0	0	8	0	9	4
9	0	0	8	0	11	3
10	0	0	8	0	2	8
10	0	0	8	0	4	7
10	0	0	8	0	6	6
10	0	0	8	0	8	5
10	0	0	8	0	10	4
10	0	0	8	0	12	3
10	0	0	8	0	14	2
11	0	0	8	0	3	8
11	0	0	8	0	5	7
11	0	0	8	0	7	6
11	0	0	8	0	9	5
11	0	0	8	0	11	4
11	0	0	8	0	13	3
11	0	0	8	0	15	2
11	0	0	8	0	17	1
12	0	0	8	0	4	8
12	0	0	8	0	6	7
12	0	0	8	0	8	6
12	0	0	8	0	10	5
12	0	0	8	0	12	4
12	0	0	8	0	14	3
12	0	0	8	0	16	2
12	0	0	8	0	18	1
12	0	0	8	0	20	0
13	0	0	8	0	11	5
13	0	0	8	0	13	4
13	0	0	8	0	15	3
13	0	0	8	0	17	2
13	0	0	8	0	19	1
14	0	0	8	0	18	2
14	0	0	8	0	20	1
14	0	0	8	0	22	0

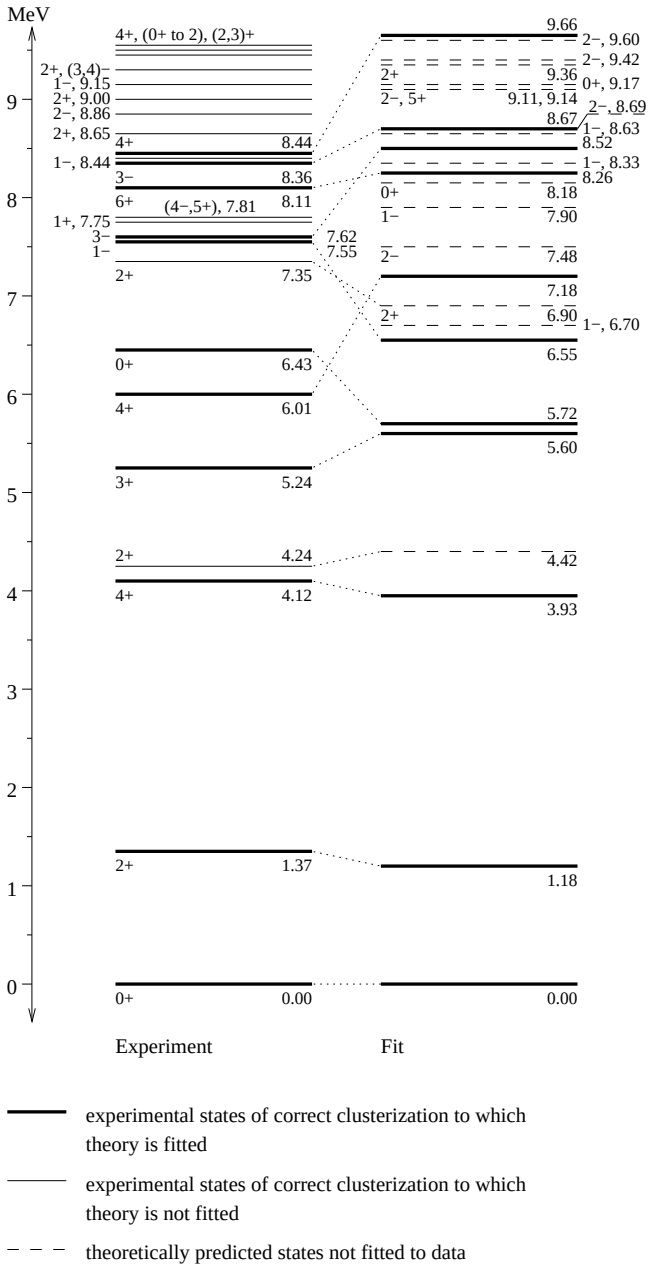

Fig. 3 – The experimental ^{24}Mg spectrum, and that calculated from SACM evaluation of the ^{20}Ne+α system.

Table 5.

^{20}Ne+α spectrum data: state spin-parity, experimental energy, and fit energy; followed by $B(E2)$ data: initial state spin-parity, final state spin-parity, experimental transition value, and fit transition value.

J^π	$E_{exp.}$ (MeV)	E_{fit} (MeV)
0_1^+	0.000	0.000
0_2^+	6.433	5.723
2_1^+	1.369	1.180
3_1^+	5.235	5.603
4_1^+	4.123	3.932
4_2^+	6.01	7.176
4_3^+	8.439	9.656
6_1^+	8.113	8.258
1_1^-	7.555	6.552
3_1^-	7.616	8.518
3_2^-	8.358	8.665

J_i^π	J_f^π	$B(E2)_{exp.}$ (W.u.)	$B(E2)_{fit}$ (W.u.)
2_1^+	0_1^+	21.5	16.89
2_2^+	2_1^+	3.6	3.96

The index γ runs over the first and second cluster and the relative part, $\boldsymbol{Q}^{(2)}_{\gamma,m}$ is the quadrupole operator of the part referred to as γ (γ = C_1, C_2, or R).

The effective charges can be estimated by applying a geometrical mapping, which involves a particular trial state (see also the Appendix). The mapping will be discussed in more detail in Section IV, using also the results of [21]. Here, we have only to assume that a trial state is used whose expectation values with respect to algebraic transition operators can be related to the geometric transition operators. For simplicity, we will assume axial symmetric deformation of the clusters.

The complete electric quadrupole operator is obtained by multiplying $\boldsymbol{T}^{(E2)}_m(\mathrm{geom})$ with p_{e2}, where "geom" refers to the geometrical estimate, *i.e.* we have $\boldsymbol{T}^{(E2)}_m = p_{e2}\boldsymbol{T}^{(E2)}_m(\mathrm{geom})$. For M1 transitions a similar procedure can be chosen. Because we do not adjust $B(M1)$ transitions, but rather calculate them directly, only the geometrical estimate is listed.

3.3.1. The electric quadrupole operator

The mapping of the individual cluster contribution is given by [21]

$$\langle \boldsymbol{Q}^{(2)}_{k,m}(\mathrm{mass})\rangle = \sqrt{\frac{5}{\pi}} N_{0,k}\alpha_{2m}(k), \tag{9}$$

($k = 1, 2$), where $N_{0,k}$ is the total number of oscillation quanta plus $\frac{3}{2}(A_k - 1)$ and A_k is the total number of nucleons in the cluster k and $\alpha_{2m}(k)$ is the geometrical

deformation variable of cluster k. Here, the quadrupole operator is still the *mass quadrupole operator*. In the numerical routine one has to multiply it by $e_k^{(2)} = \frac{Z_k}{A_k}$. The p_{e2} is an overall parameter of the total quadrupole operator and measures the deviation from the geometrical estimate.

Table 6.

Parameter values defining the ^{20}Ne+α interaction. The p_{e2} parameter is the effective charge and is explained in detail in subsection C

Hamiltonian and transition							
a	$\bar{a}$	γ	a_{Clus}	$\bar{b}$	b		
-0.136	-1.39	0.197	0.000	-0.044	-0.116		
c	a_C	$a_R^{(1)}$	t	p_{e2}			
0.0	0.0	0.0	0.811	0.306			
Symmetry mixing							
x	y						
1.0	1.0						
Clusters							
λ_1	μ_1	$N_{0,1}$	β_1	λ_2	μ_2	$N_{0,2}$	β_2
0	0	4.5	0.0	8	0	48.5	0.73
Quanta							
$\hbar\omega$	n_0	N					
12.6	8	12					

Table 7.

Phase space details of the investigated systems. Both systems lie in the region III, *i.e.* in the spherical limit, but near to the line of the second order phase transition.

System	A	B	C	Region
^{14}C+α	152.308	11.887	0	III
^{20}Ne+α	-185.826	-20.782	0	III

Comparing both sides we obtain a relation between the effective charge and the $N_{0,k}$ plus the deformation. Let us for that consider the $m = 0$ component. Then $\alpha_{20}(k)$ is in the intrinsic system just $\beta(k)$, *i.e.* the deformation parameter. The expectation of the algebraic quadrupole operator with respect to a $SU(3)$ basis is given by (with spin being two and the projection of the states being zero)

$$\begin{aligned}
&\langle(\lambda_k,\mu_k)\kappa_k = 1\, L_k = 2\, M_k = 0 \mid Q_{20} \mid (\lambda_k,\mu_k)\kappa_k = 1\, L_k = 2\, M_k = 0\rangle \\
&= \langle(\lambda_k,\mu_k)12,(1,1)12 \mid\mid (\lambda_k,\mu_k)12\rangle_1(20,20 \mid 20)2(-1)^{\phi}\sqrt{C_2(\lambda_k,\mu_k)} \\
&= Q_0(\lambda_k,\mu_k). \qquad (10)
\end{aligned}$$

The first factor refers to an isoscalar factor [22], the second factor is a $SU(2)$ Clebsch-Gordan coefficient, $C_2(\lambda,\mu) = (\lambda^2+\lambda\mu+\mu^2+3\lambda+3\mu)$ and ϕ is 1 for $\mu \neq 0$ and 0 for $\mu = 0$. The factor $2(-1)^{\phi}\sqrt{C_2(\lambda_k,\mu_k)}$ is the triple reduced matrix element of the quadrupole operator, which is a generator of $SU(3)$ [22].

We obtain then for the effective charge

$$e_k^{(2)} = \sqrt{\frac{5}{\pi}} N_{0,k}\beta_{0,k}/Q_0(\lambda_k,\mu_k). \tag{11}$$

The radial part can be readily copied from [21], taking the limit for $N >> 1$. We obtain

$$\langle e_R^{(2)} \boldsymbol{Q}_{R,m}^{(2)} \rangle \approx \sqrt{6} e_R^{(2)} N \left[\alpha \times \alpha\right]_m^{[2]}. \tag{12}$$

(Note that we used the definition $\boldsymbol{Q}_{R,m}^{(2)} = \sqrt{6}\left[\pi^{\dagger} \times \tilde{\pi}\right]_m^{[2]}$, *i.e.*, with a $\sqrt{6}$ factor instead of $\frac{\sqrt{3}}{2}$ as it was used in [5, 6]. The definition used by us is more in line with the physical definition of the quadrupole operators, where the $m = 0$ part has to be given by $(2z^2 - x^2 - y^2)$, for the part depending on the coordinates, and similar for the momentum part.) Using [21] we obtain

$$\alpha_m \approx \sqrt{\frac{\mu\omega_r}{2N\hbar}}(r_m - r_{0,m}), \tag{13}$$

where μ is the reduced mass and $\omega_r = \sqrt{\frac{A_1+A_2}{A_1A_2}}\omega$ [23]. (This strange number comes from the consideration that the oscillator constant $m\omega^2$ changes after a transformation in the radial part to $\mu\omega_r^2$ with the condition that both stay the same; it is an orthogonal transformation and this consideration was forgotten in [21].) We started from a quadrupole operator without units. In order to obtain the correct effective charge, we have still to multiply by $(\frac{\hbar}{m\omega})$, using for the moment and for convenience $r_{0,m} = 0$, we arrive at

$$\sqrt{6} e_R^{(2)} \frac{\mu\omega_r}{2m\omega} \left[r \times r\right]_m^{[2]}. \tag{14}$$

This has to be compared to the classical definition of the quadrupole operators. The $m = 0$ component is given by $(2z^2 - x^2 - y^2)$ which in spherical components has the form $2(r_0^2 + r_+ r_-)$. Comparing this with the expectation value we can depict $e_R^{(2)}$ and the result is

$$e_R^{(2)} = 2\frac{m\omega}{\mu\omega_r}. \tag{15}$$

The factor of 2 is the usual effective charge. In [5, 6] the algebraic operator has no units, *i.e.* these units have to be carried by the effective charge.

3.3.2. The magnetic dipole transition operator

The $M1$ operator is defined as

$$\boldsymbol{T}^{(M1)} = \mu_0 \left(g_1 \boldsymbol{L}_m^{(1)} + g_2 \boldsymbol{L}_m^{(2)} + g_R \boldsymbol{L}_R \right). \tag{16}$$

The gyromagnetic factors are given by $g_k = \frac{Z_k}{A_k}$ [24] and the one of the radial motion is $\frac{Z}{A}$.

The factors in (16) at the same time give an expression for the effective charges in front of the angular momentum operators, *i.e.*

$$e_k^{(1)} = \mu_0 \frac{Z_k}{A_k}, \qquad e_R^{(1)} = \mu_0 \frac{Z}{A}. \tag{17}$$

In the case of magnetic dipole transitions, no extra parameter appears, which shows the deviations from this geometrical estimate to experiment. The reason is that no magnetic dipole transition was used in the fit.

3.3.3. Numerical results

The numerical values of the $B(E2)$ and $B(M1)$ values for the systems considered are listed in tables 8 to 9.

There are, however, transitions which yield zero in the SACM, while they are not zero in experiment. In the SACM these transitions are zero because the states belong to different $SU(3)$ irreducible representations, which can be deduced from Tables 10 to 13. The exception seems to be the $B(E2; 2_2^+ \to 2_1^+)$ transition in ^{20}Ne+α, but these states belong to different multiplicity labels, though the $SU(3)$ irrep is the same. Due to the different multiplicity labels, these states can not be connected. There the experimental value is also very low, which indicates that the $SU(3)$ limit explains this behavior.

In ^{20}Ne+α the agreement to experiment is remarkably good, referring to the energy levels and the transition data. Some transition data are zero, while in experiment these are not. The reason is that the transitions which are zero correspond to states in different $SU(3)$ irreducible representations and can not be connected by the algebraic quadrupole operator. One possibility is to include in the fit transitions which are between different $SU(3)$ irreps and force the system to deviate from the $SU(3)$ dynamical limit. The good agreement suggest that the calculated α-spectroscopic factors are of confidence.

The situation is somewhat different in ^{14}C+α: In ^{14}C+α the 2_3^+ to 4_1^+ and the 2_3^+ to 0_2^+ transitions are extremely strong compared to the ground state band transitions. These data indicate that the 0_2^+, 2_3^+ and 4_1^+ states belong to the same band *and* these states are much more deformed than the ones in the 0_1^+ and 2_1^+ states. This implies an exited band in a different minimum, which can not be reproduced within

the SACM, except when further interaction terms are taken into account. These additional low lying states of different deformation suggest to our fitting routine a denser spectrum at low energy in the minimum where the ground state is, which explains the many states which have no experimental equivalence. Therefore, one has to take with *a grain of salt* the results presented for the α-spectroscopic factors and further studies, including a stronger mixing in SU(3), have to be applied. One possibility is to include in the fit transitions which are zero in the pure $SU(3)$ dynamical limit but not zero in experiment. Probably, further interaction terms also have to be included, which produce a second local deformed minimum (in the geometrical mapping) at higher energy.

The correction, p_{e2}, to the effective charge of the quadrupole is in both systems of the order of 0.3. This indicates that the geometrical estimate is off by about a factor three.

Table 8.

$B(E2)$ and $B(M1)$ values for the system ^{14}C+α, compared to experiment where available. The type is 2 for $E2$ transitions and 3 for $M1$ transitions. The $L_i(q_i)$ refers to the initial angular momentum of the $q_i{}^{\mathrm{th}}$ state and $L_f(q_f)$ refers to the final state of the $q_f{}^{\mathrm{th}}$ state. In the column, denoted as "value", the transition value is given, where the units are given in WU (Weisskopf units). The experimental data are from [19].

type	$L_i(q_i)$	$L_f(q_f)$	value	exp.
2	2_1^+	0_1^+	3.74	3.32
2	0_2^+	2_1^+	0	17
2	2_2^+	0_1^+	1.19	1.3
2	2_3^+	0_2^+	0.143	23
2	2_3^+	4_1^+	0	21
2	2_3^+	0_1^+	0	2.15
2	4_1^+	2_1^+	4.98	1.19
2	4_2^+	2_2^+	1.826	2.2
2	2_4^+	4_1^+	0	2.4
2	0_3^+	2_1^+	0	2.0
3	2_2^+	2_1^+	0.0009	0.14
3	2_3^+	2_2^+	0	0.111

3.4. SPECTROSCOPIC FACTORS

Within the SACM, the first attempt to calculate the spectroscopic factors was published in [25] and applied to nuclei in the p and sd shell. A polynomial ansatz for the operator was used, which provides the spectroscopic factors. In [26] an exponential ansatz was proposed and theoretical spectroscopic factors for cluster radioactivity [14] were obtained. The spectroscopic factor, as a function of the mass of the

Table 9.

$B(E2)$ and $B(M1)$ values for the system ^{20}Ne+α, compared to experiment, if available. The type is 2 for $E2$ transitions and 3 for $M1$ transitions. The $L_i(q_i)$ refers to the initial angular momentum of the q_i^{th} state and $L_f(q_i)$ refers to the final state of the q_i^{th} state. In the column, denoted as "value", the transition value is given, where the units are given in WU (Weisskopf units). The experimental data are taken from [20].

type	$L_i(q_i)$	$L_f(q_f)$	value	exp.
2	2_1^+	0_1^+	16.89	21.5
2	4_1^+	2_1^+	22.69	39
2	2_2^+	2_1^+	3.96	3.15
2	0_2^+	2_2^+	0	8.9
2	0_2^+	2_1^+	0	0.64
2	2_2^+	0_1^+	2.107	1.94
2	3_1^+	2_1^+	3.763	2.5
2	3_1^+	2_2^+	30.157	58
2	2_3^+	0_1^+	0	0.67
3	2_2^+	2_1^+	0	9.00E-06
3	3_1^+	2_1^+	1.28E-31	2.10E-05
3	3_1^+	2_2^+	1.69E-31	0.00035
3	1_1^+	0_1+	0.	0.00078

emitted cluster, was calculated, extending the simple method proposed in [27]. This new parametrization was applied in [28] to the total cross section of ^{12}C+^{12}C, with remarkable success, such that even some resonance structure is recreated.

Finally, in [29] the exponential ansatz of [26] was augmented by isoscalar factors and the parameters were fitted, mainly to states in cluster plus α systems within the sd shell, *i.e.*, just the systems considered in this contribution. The mentioned ansatz of the operator for the spectroscopic factor is

$$\begin{aligned} S = &\exp\big\{A + Bn_\pi + C\mathcal{C}_2(\lambda_1,\mu_1) + D\mathcal{C}_2(\lambda_2,\mu_2) \\ &+ E\mathcal{C}_2(\lambda_c,\mu_c) + F\mathcal{C}_2(\lambda,\mu) + G\mathcal{C}_3(\lambda,\mu) + H\Delta n_\pi\big\} \\ &\times |\,\langle(\lambda_1,\mu_1)\kappa_1 L_1,(\lambda_2,\mu_2)\kappa_2 L_2||(\lambda_C,\mu_C)\kappa_C L_C\rangle_{\rho_C} \\ &\langle(\lambda_C,\mu_C)\kappa_C L_C,(n_\pi,0)1L_R||(\lambda,\mu)\kappa L\rangle_1\,|^2, \end{aligned} \tag{18}$$

where $\mathcal{C}_3(\lambda,\mu)$ is the third order Casimir operator of $SU(3)$ with eigenvalue $(\lambda-\mu)(2\lambda+\mu+3)(\lambda+2\mu+3)$, which is important in order to distinguish excited states like (λ,μ) and (μ,λ). The $\mathcal{C}_2(\lambda_k,\mu_k)$ $(k=1,2,C)$ is the second order Casimir operator with eigenvalue $(\lambda_k^2+\lambda_k\mu_k+\mu_k^2+3\lambda_k+3\mu_k)$. Finally, Δn_π = $(n_\pi - n_o)$ gives the difference in the number of relative quanta in excited states to the number in the ground state, which is determined by the Wildermuth condition and L_R is the angular momentum of the relative motion. This formula is only valid for even-even nuclei, to which we restrict ourselves here.

Table 10.

List of spectroscopic factors (S) and energies of states with positive parity, for the system ^{14}C+α. The 1_5^+ state is not listed because it is over 50 MeV.

(λ_C,μ_C)	n_π	(λ,μ)	L_k^π	E[MeV]	S
$(0,2)$	8	$(8,2)$	0_1^+	0.000	0.185
$(0,2)$	6	$(4,0)$	0_2^+	3.592	0.206
$(0,2)$	10	$(10,2)$	0_3^+	6.324	0.094
$(0,2)$		$(6,0)$	0_4^+	8.254	0.111
$(0,2)$	10	$(8,0)$	0_5^+	11.555	0.064
$(0,2)$	10	$(9,1)$	1_1^+	10.438	0.125
$(0,2)$	12	$(11,1)$	1_2^+	16.300	0.057
$(0,2)$	14	$(13,1)$	1_3^+	25.230	0.025
$(0,2)$	16	$(15,1)$	1_4^+	39.053	0.011
$(0,2)$		$(8,2)$	2_1^+	1.173	0.180
$(0,2)$	8	$(8,2)$	2_2^+	4.730	0.00009
$(0,2)$	6	$(4,0)$	2_3^+	4.765	0.177
$(0,2)$	10	$(10,2)$	2_4^+	7.497	0.093
$(0,2)$	8	$(6,0)$	2_5^+	9.427	0.101
$(0,2)$	8	$(8,2)$	3_1^+	5.903	0.176
$(0,2)$	10	$(10,2)$	3_2^+	12.227	0.091
$(0,2)$	10	$(9,1)$	3_3^+	12.393	0.124
$(0,2)$	12	$(11,1)$	3_4^+	18.255	0.056
$(0,2)$	12	$(12,2)$	3_5^+	20.574	0.040
$(0,2)$	8	$(8,2)$	4_1^+	3.910	0.168
$(0,2)$	8	$(8,2)$	4_2^+	7.467	0.002
$(0,2)$	6	$(4,0)$	4_3^+	7.502	0.108
$(0,2)$	10	$(10,2)$	4_4^+	10.234	0.088
$(0,2)$	8	$(6,0)$	4_5^+	20.574	0.080
$(0,2)$	8	$(8,2)$	5_1^+	9.422	0.173
$(0,2)$	10	$(10,2)$	5_2^+	15.746	0.089
$(0,2)$	10	$(9,1)$	5_3^+	15.912	0.122
$(0,2)$	12	$(11,1)$	5_4^+	21.774	0.055
$(0,2)$	12	$(12,2)$	5_5^+	24.093	0.039
$(0,2)$	8	$(8,2)$	6_1^+	8.211	0.145
$(0,2)$	8	$(8,2)$	6_2^+	11.768	0.008
$(0,2)$	10	$(10,2)$	6_3^+	14.535	0.046
$(0,2)$	8	$(6,0)$	6_4^+	16.464	0.032
$(0,2)$	10	$(10,2)$	6_5^+	18.092	0.002

Table 11.

List of spectroscopic factors (S) and energies of states with negative parity, for the system ^{14}C+α

(λ_C,μ_C)	n_π	(λ,μ)	L_k^π	E[MeV]	S
$(0,2)$	7	$(6,1)$	1_1^-	3.407	0.007
$(0,2)$	9	$(9,2)$	1_2^-	3.414	0.135
$(0,2)$	7	$(5,0)$	1_3^-	6.598	0.130
$(0,2)$	9	$(8,1)$	1_4^-	8.087	0.003
$(0,2)$	9	$(7,0)$	1_5^-	10.351	0.085
$(0,2)$	7	$(6,1)$	2_1^-	4.189	0.298
$(0,2)$	9	$(9,2)$	2_2^-	7.753	0.131
$(0,2)$	9	$(8,1)$	2_3^-	8.869	0.175
$(0,2)$	11	$(10,1)$	2_4^-	13.881	0.085
$(0,2)$	11	$(11,2)$	2_5^-	14.861	0.061
$(0,2)$	7	$(6,1)$	3_1^-	5.362	0.043
$(0,2)$	9	$(9,2)$	3_2^-	5.269	0.130
$(0,2)$	7	$(5,0)$	3_3^-	8.553	0.106
$(0,2)$	9	$(9,2)$	3_4^-	8.926	0.0002
$(0,2)$	9	$(8,1)$	3_5^-	10.042	0.017
$(0,2)$	7	$(6,1)$	4_1^-	6.926	0.294
$(0,2)$	9	$(9,2)$	4_2^-	10.490	0.129
$(0,2)$	9	$(8,1)$	4_3^-	11.606	0.173
$(0,2)$	11	$(10,1)$	4_4^-	16.618	0.084
$(0,2)$	11	$(11,2)$	4_5^-	17.598	0.061
$(0,2)$	7	$(6,1)$	5_1^-	8.881	0.106
$(0,2)$	9	$(9,2)$	5_2^-	8.888	0.120
$(0,2)$	7	$(5,0)$	5_3^-	12.072	0.062
$(0,2)$	9	$(9,2)$	5_4^-	12.445	0.002
$(0,2)$	9	$(8,1)$	5_5^-	13.561	0.042
$(0,2)$	7	$(6,1)$	6_1^-	11.227	0.287
$(0,2)$	9	$(9,2)$	6_2^-	14.791	0.126
$(0,2)$	9	$(8,1)$	6_3^-	15.907	0.179
$(0,2)$	11	$(10,1)$	6_4^-	20.919	0.082
$(0,2)$	11	$(11,2)$	6_5^-	21.899	0.059

The parameters were adjusted to 17 states of a cluster plus α systems [29]. The values of the fitted parameters are $A = 2.1466$, $B = -0.36113$, $C = -0.054389$, $D = -0.11764$, $E = 0.060728$, $F = -0.0086654$, $G = 0.000021097$ and $H = 1.90901$. The parameter A was chosen in [29] such that it gives 1 for the ground state of ^{16}O+α. Here we changed it in order to reproduce the absolute value of 0.23, as given by the microscopic calculation of [30]. The spectroscopic factors of about 100 further states were calculated, with an excellent agreement within a couple of percent to $SU(3)$ microscopic calculations (for references, please consult [29]). Mainly cluster plus α states were considered, though, also some 15 states were included which refer to ^{12}C+^{12}C and ^{16}O+^{8}Be. The same parametrization was used with success in [26], where spectroscopic factors of cluster radioactivities were calculated, and in [12] where the ^{18}Ne(α,p)^{21}Na reaction was investigated, a system which is of astrophysical importance.

The structure of the spectroscopic factor can be understood by the following argument: The probability of finding two clusters at a distance R from one another is proportional to $|F(R)|^2$ [11], where $F(R) \sim exp(-aR^2)$ is the relative motion wave function. On the other hand the expectation value of R satisfies $\langle R \rangle \sim \sqrt{n_\pi}$ when the SACM is mapped onto a geometrical picture [31] and this results in the n_π dependence in the exponent. From this consideration one expects a negative value for the parameter $B = -a$. The eigenvalues of the Casimir operators of the $SU(3)$ groups are proportional to the square of the deformation [32, 33]. A larger deformation corresponds to a more extended system and thus is also related to the relative distance of the clusters. The $SU_C(3)$ group describes the relative orientation of the nuclei [31] and large eigenvalue of the corresponding Casimir operator are related to an orientation which is less compact (more prolate), *i.e.*, one can consider these contributions as corrections to the overlap. Of course, these explanations are of hand waving nature only and a more thorough understanding is required.

There is, however, a problem related to the expression in (18): When Δn_π is large, the argument of the exponential gets large and as a result spectroscopic factors with values much larger than one are obtained. We propose here a modification of this expression, such that for Δn_π = 0 1, and 2 the results are *identical* to [29], but for large Δn_π the argument goes to zero, *i.e.*, the exponential factor tends to one and the only variation is due to the isoscalar factors. Because the results are identical to [29], where only states with Δn_π = 0 and 2 were adjusted, the same parameter values can be used. Of course, the new proposal is an *interpolation* to higher n_π and represents a *model* rather than a theory.

The new ansatz for the spectroscopic factor, which interpolates between the low n_π to large n_π, is given by

$$S = \exp(F_1 + F_2) \times |< (\lambda_1,\mu_1)\kappa_1 L_1, (\lambda_2,\mu_2)\kappa_2 L_2 || (\lambda_C,\mu_C)\kappa_C L_C >_{\rho_C} < (\lambda_C,\mu_C)\kappa_C L_C, (n_\pi,0) 1 L_R || (\lambda,\mu)\kappa L >_1 |^2, \quad (19)$$

where

$$F_1 = A + B n_\pi + C\mathcal{C}_2(\lambda_1,\mu_1) + D\mathcal{C}_2(\lambda_2,\mu_2) + E\mathcal{C}_2(\lambda_c,\mu_c) + F\mathcal{C}_2(\lambda,\mu) + G\mathcal{C}_3(\lambda,\mu) \quad (20)$$

and

$$F_2 = -F_1 \frac{\Delta n_\pi(\Delta n_\pi - 1)(\Delta n_\pi - 2)}{n_\pi^3} + H \frac{(n_0+2)^3(\Delta n_\pi - 1)}{n_\pi^4} \frac{\Delta n_\pi}{n_\pi}. \quad (21)$$

The expressions for the spectroscopic factor in (18) and (19) are diagonal in a $SU(3)$ basis, which is the reason that it is not written in terms of operators. When mixing is included, the spectroscopic factors calculated will also deviate from $SU(3)$. Because the systems considered turned out to be best described within the $SU(3)$ dynamical symmetry limit, the calculates spectroscopic factors are those of $SU(3)$, using the approximation of [29], which give a very good approximation for the $SU(3)$ spectroscopic factors. Note that the experimental extraction of spectroscopic factors often use the *Distorted Wave Born Approximation* (DWBA), *i.e.* it is also model dependent. In practice the numerical values can deviate from the $SU(3)$ ones by several factors, *i.e.*, a deviation by a large factor does not mean that our results give a poor agreement.

Because of the success of this model, we present here the numerical values of the systems considered in this publication. The results are listed in Tables 10 to 13 for the two systems ^{14}C+α and ^{20}Ne+α respectively. In [34] some spectroscopic factors in the ^{14}C+α system were experimentally determined, using the ratio of the measured partial cross section to the one in the DWBA model. In Table 14 we list these values compared to our model, where the experimental states have been assigned to certain theoretical states. Some ambiguity exist in the 5_1^- and 5_2^-, which in theory are practical degenerate. In Table 14 only the first state is listed. As can be seen, even when we have some problems in reproducing the spectrum at low energy, due to the appearance of large deformed states, the agreement for the spectroscopic factors in the states listed is remarkable good. Of course, one has to take it with a grain of salt, due to the difficulties in this system, mentioned before.

4. GEOMETRICAL INTERPRETATION OF RESULTS.

In another recent paper [2], a detailed investigation of the phase space of the SACM was presented. Potentials were formed by taking the expectation value of the

Table 12.

List of spectroscopic factors (S) and energies of states with positive parity, for the system ^{20}Ne+α.

(λ_C,μ_C)	n_π	(λ,μ)	L^π_k	E[MeV]	S
$(8,0)$	8	$(8,4)$	0^+_1	0.000	0.050
$(8,0)$	8	$(4,6)$	0^+_2	5.723	0.068
$(8,0)$	8	$(8,0)$	0^+_3	8.176	0.062
$(8,0)$	10	$(2,8)$	0^+_4	9.175	0.040
$(8,0)$	10	$(6,6)$	0^+_5	12.056	0.028
$(8,0)$	10	$(4,7)$	1^+_1	10.720	0.027
$(8,0)$	10	$(8,5)$	1^+_2	15.565	0.020
$(8,0)$	10	$(12,3)$	1^+_3	21.903	0.012
$(8,0)$	12	$(6,7)$	1^+_4	28.871	0.015
$(8,0)$	12	$(10,5)$	1^+_5	47.412	0.010
$(8,0)$	8	$(8,4)$	2^+_1	1.180	0.019
$(8,0)$	8	$(8,4)$	2^+_2	4.424	0.002
$(8,0)$	8	$(4,6)$	2^+_3	6.903	0.017
$(8,0)$	8	$(8,0)$	2^+_4	9.356	0.015
$(8,0)$	8	$(4,6)$	2^+_5	10.147	0.003
$(8,0)$	8	$(8,4)$	3^+_1	5.603	0.025
$(8,0)$	8	$(4,6)$	3^+_2	11.327	0.048
$(8,0)$	8	$(8,4)$	3^+_3	12.686	0.024
$(8,0)$	8	$(4,6)$	3^+_4	14.778	0.026
$(8,0)$	10	$(4,7)$	3^+_5	15.930	0.00004
$(8,0)$	10	$(2,8)$	4^+_1	3.932	0.00006
$(8,0)$	10	$(4,7)$	4^+_2	7.176	0.023
$(8,0)$	8	$(8,4)$	4^+_3	9.656	0.010
$(8,0)$	8	$(8,4)$	4^+_4	12.109	0.009
$(8,0)$	8	$(4,6)$	4^+_5	12.900	0.0004
$(8,0)$	8	$(8,0)$	5^+_1	9.143	0.024
$(8,0)$	8	$(4,6)$	5^+_2	14.866	0.033
$(8,0)$	8	$(8,4)$	5^+_3	16.226	0.016
$(8,0)$	8	$(4,6)$	5^+_4	18.317	0.018
$(8,0)$	10	$(4,7)$	5^+_5	18.875	0.0009
$(8,0)$	10	$(2,8)$	6^+_1	8.258	0.007
$(8,0)$	8	$(8,4)$	6^+_2	11.502	0.035
$(8,0)$	8	$(8,4)$	6^+_3	13.981	0.007
$(8,0)$	8	$(4,6)$	6^+_4	16.434	0.006
$(8,0)$	8	$(8,0)$	6^+_5	17.225	0.0002

Table 13.

List of spectroscopic factors (S) and energies of states with negative parity, for the system ^{20}Ne+α.

(λ_C,μ_C)	n_π	(λ,μ)	L_k^π	E[MeV]	S
$(8,0)$	8	$(4,6)$	1_1^-	6.552	0.022
$(8,0)$	9	$(9,4)$	1_2^-	6.699	0.004
$(8,0)$	9	$(7,5)$	1_3^-	7.906	0.009
$(8,0)$	9	$(5,6)$	1_4^-	8.329	0.029
$(8,0)$	9	$(3,7)$	1_5^-	8.631	0.013
$(8,0)$	9	$(11,3)$	2_1^-	7.486	0.0009
$(8,0)$	9	$(7,5)$	2_2^-	8.693	0.001
$(8,0)$	9	$(5,6)$	2_3^-	9.115	0.002
$(8,0)$	9	$(3,7)$	2_4^-	9.417	0.002
$(8,0)$	9	$(1,8)$	2_5^-	9.598	0.002
$(8,0)$	9	$(9,4)$	3_1^-	8.518	0.005
$(8,0)$	9	$(11,3)$	3_2^-	8.665	0.015
$(8,0)$	9	$(7,5)$	3_3^-	9.873	0.026
$(8,0)$	9	$(5,6)$	3_4^-	10.295	0.011
$(8,0)$	9	$(3,7)$	3_5^-	10.597	0.005
$(8,0)$	9	$(11,3)$	4_1^-	10.238	0.005
$(8,0)$	9	$(7,5)$	4_2^-	11.446	0.007
$(8,0)$	9	$(5,6)$	4_3^-	11.868	0.009
$(8,0)$	9	$(3,7)$	4_4^-	12.170	0.010
$(8,0)$	9	$(1,8)$	4_5^-	12.351	0.010
$(8,0)$	9	$(9,4)$	5_1^-	12.057	0.0006
$(8,0)$	9	$(11,3)$	5_2^-	12.205	0.014
$(8,0)$	9	$(7,5)$	5_3^-	13.412	0.010
$(8,0)$	9	$(5,6)$	5_4^-	13.834	0.006
$(8,0)$	9	$(3,7)$	5_5^-	14.136	0.004
$(8,0)$	9	$(11,3)$	6_1^-	14.564	0.010
$(8,0)$	9	$(7,5)$	6_2^-	15.771	0.015
$(8,0)$	9	$(5,6)$	6_3^-	16.194	0.017
$(8,0)$	9	$(3,7)$	6_4^-	16.495	0.019
$(8,0)$	9	$(1,8)$	6_5^-	16.676	0.021

Table 14.

Some spectroscopic factors for states in ^{14}C+α, compare to those determined in experiment.

L_k^π	$E_{\rm theo}$ [MeV]	$E_{\rm exp}$ [MeV]	$S_{\rm theo}$	$S_{\rm exp}$
5_1^-	8.88	8.120	0.11	0.09
6_1^-	11.23	11.06	0.29	0.27
6_2^-	14.79	14.1	0.13	0.16
6_3^-	15.91	14.3	0.16	0.05

Hamiltonian with the SACM coherent states, defined as

$$\begin{aligned} |\alpha\rangle &= \mathcal{N}_{N,n_0}(\boldsymbol{\alpha}\cdot\boldsymbol{\pi})^{n_0}\left[\boldsymbol{\sigma}^\dagger+\left(\boldsymbol{\alpha}\cdot\boldsymbol{\pi}^\dagger\right)\right]^N|0\rangle \\ &= \mathcal{N}_{N,n_0}\frac{N!}{(N+n_0)!}\times\frac{d^{n_0}}{d\gamma_1^{n_0}}\left[\boldsymbol{\sigma}^\dagger+\gamma_1\left(\boldsymbol{\alpha}\cdot\boldsymbol{\pi}^\dagger\right)\right]^{N+n_0}|0\rangle\,, \end{aligned} \tag{22}$$

where, for convenience, we redefined the total number of relative oscillation quanta as $(N+n_0)$ and the γ_1 parameter has to be set equal to 1 after the differentiation. The $\mathcal{N}_{N,n_0}$ is an appropriate normalization factor [2, 31].

The geometrical mapped potential is then obtained by the expectation value

$$V(\alpha)=\langle\boldsymbol{\alpha}|\,\boldsymbol{H}\,|\boldsymbol{\alpha}\rangle\,. \tag{23}$$

The α can be related to the distance between the clusters [21]. It is proportional to $(r-r_0)/\sqrt{N}$, where r is the radial distance and r_0 is proportional to $\sqrt{n_0}$. In a model with no Pauli principle included, α is therefore directly proportional to the distance between the two clusters. One denotes than the *spherical limit* as the one with $\alpha=0$ and the *deformed limit* when $\alpha>0$. However, when the Pauli exclusion principle is taken into account, which is the case in the SACM, there is always a minimal distance r_0 between the two clusters, due to the minimal number, n_0, of relative oscillation quanta. Nevertheless, the notation of *spherical* and *deformed limit* is maintained, even if for $\alpha=0$ the $r>0$.

Explicit expressions for the potential can be found in [2, 3]. Due to the implementation of the minimal number of quanta, *i.e.* $n_0>0$, the expressions are quite complicated and involve ratios of polynomials in the variable α. Explicit expressions and their limit for $\alpha\to\infty$ are given in the Appendix. Just to give an impression, the structure of the potential can be written in the form

$$V=-xyb\left(A\alpha^2\frac{F_{11}(\alpha^2)}{F_{00}(\alpha^2)}-B\alpha^4\frac{F_{22}(\alpha^2)}{F_{00}(\alpha^2)}+\alpha^6\frac{F_{22}(\alpha^2)}{F_{00}(\alpha^2)}-C\alpha^2\frac{F_{20}^{N-2}(\alpha^2)}{F_{00}(\alpha^2)}\right)+D, \tag{24}$$

where A, B, C and D are linearly-independent parameters, which in turn dependent on all parameters of the Hamiltonian and on n_0 and N. (They are not to be confused with the parameters of Eq.(18).) The functions F_{ij} dependent on α, n_0 and N. More details are to be published elsewhere [3]. Again, the α-dependent component of V in (24) is sufficient for studying phase transitions. Note that even if the Hamiltonian depends on many parameters, we can reduce the discussion of phase transitions to only three effective parameters. The potential (24) can exhibit only one deformed, or one spherical, or two potential minima, where at one is spherical. When at the point of phase transition the two minima are at different values of α, the order of the phase transition is one, while it is of the order of two when the two potentials merge at the point of phase transition [3].

When the Pauli exclusion principle is not taken into account ($n_0 = 0$, the ratios of the $F_{kq}(\alpha^2)$ functions are extremely simple. The structure of (24) can also be reproduced by such kind of models, but with the expense of including ratios of polynomial interactions of high order. This effect was also observed in the treatment of heavy ion collisions, where in the relative motion the potential should exhibit a repulsive potential for smaller relative distances. The terms in (24) are nothing but the results of the repulsion between the fermions (nucleons), *i.e.*, the existence of the Pauli exclusion principle.

In Fig. 4 structure of the phase space for the general problem is shown, though the exact position of the surface shown still depends on n_0 (due to the dependence of the $F_{pq}(\alpha^2)$ functions in the potential, which depend on n_0). There is a second order phase transition when $C > 0$. At $C = 0$, indicated by the solid line, the second order phase transition turns over into a first order phase transition. This first order phase transition is continued up to approximately $C = -15$, indicated by the dashed line. For more negative C there is no phase transition, *i.e.*, the dashed line constitutes a *critical line* around which one can develop a system without experiencing a phase transition. This is quite new, because in standard algebraic cluster models no Pauli exclusion principle is taken into account and only interactions up to second order are considered. With these restrictions, only second order phase transitions occur [35].

There are five different regions, called by us Region 0 to IV: Region I corresponds to the existence of two minima where the deformed one is the global minimum. Region II also corresponds to two minima where the deformed one is the global minimum. In Region III there is only one spherical minimum and in region IV there is only one deformed minimum. Region 0 is the case where there are no minima whatsoever, with the system being entirely unbound. (Potentials therein have the shape of the negative of the potentials seen in Fig. 6.)

The parameter values for the two cases considered are given in Table 7. In Fig. 5, a section of the phase space diagram is shown for the two systems. The left panel corresponds to ^{14}C+α while the right panel corresponds to ^{20}Ne+α. The dot indicates where the system lies with respect to the the surface of phase transitions. According to that and using the notation as given before, ^{18}O and ^{24}Mg are in the region of a spherical potential.

In Fig. 6 the potential of the two systems is plotted. The left panel shows the result for the ^{14}C+α system and the right panel for the ^{20}Ne+α system. Both exhibit a spherical minimum, in the sense that it is at $\alpha = 0$. Note that in the SACM this still corresponds to a separation proportional to $\sqrt{n_0}$, as mentioned before.

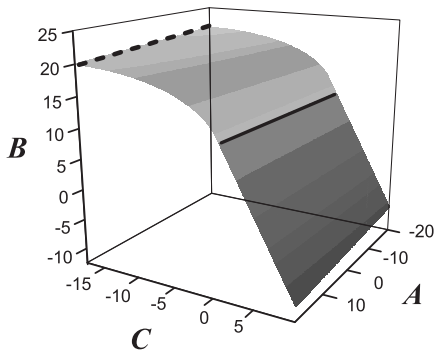

Fig. 4 – The phase space as a function of the three parameters A, B and C. The surface from the right to the left, until the solid line, represents phase transition of the second order. The surface to the left of the solid line correspond to phase transitions of first order. After $C \lesssim -15$ there is no phase transition present, *i.e.* the line at $C \lesssim -15$ is a *critical line*.

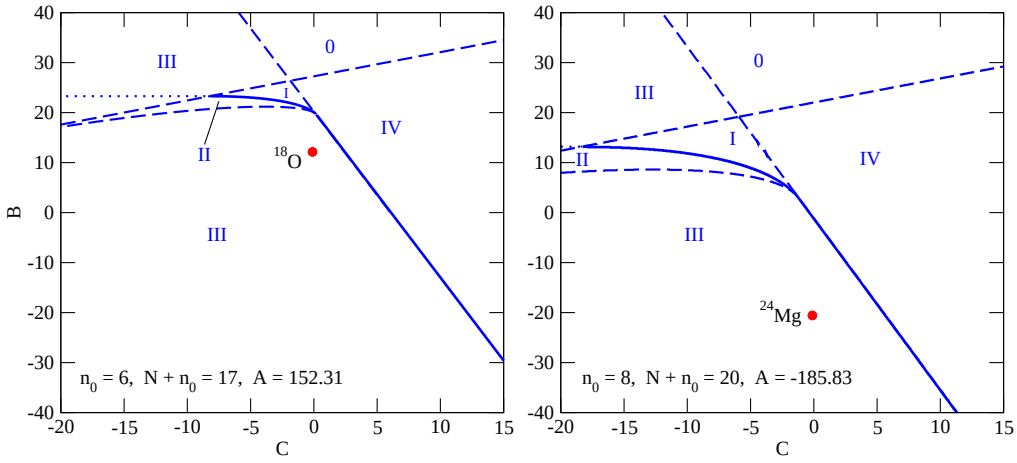

Fig. 5 – A small section of the phase space diagram given in Fig. 4. The left panel corresponds to ^{14}C+α and the right panel to ^{20}Ne+α. The dot indicates the location of the system relative to the surface of the second order phase transition.

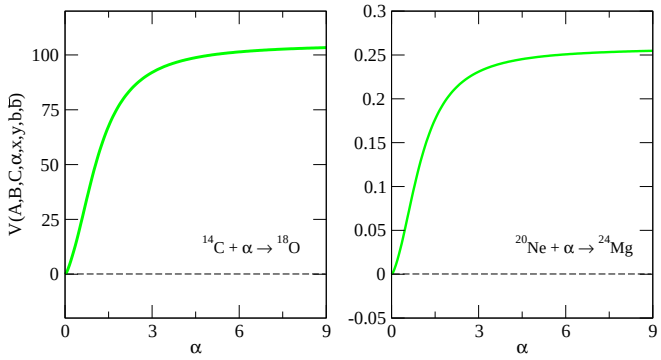

Fig. 6 – The potentials corresponding to the two systems ^{12}C+α (left panel) and ^{20}Ne+α (right panel), respectively.

5. CONCLUSIONS

In this contribution we applied the *Semimicroscopic Algebraic Cluster Model* (SACM) [5, 6] to two cluster systems of astrophysical interest. We consider two-cluster systems where one is an α-particle. The systems considered were ^{14}C+α and ^{20}Ne+α, corresponding to ^{18}O and ^{24}Mg, respectively.

Energies and $B(E2)$-values were adjusted. The complete spectrum and a list of $B(E2)$-, $B(M1)$-values and of spectroscopic factors were calculated. The adjusted spectrum and transition values show that the SACM is capable of reproducing experimental data quite well. The spectroscopic factors were not adjusted and represent a prediction of the SACM.

Also the geometrical mapping was discussed and the position of the systems considered, within the phase space diagram. According to this, both systems are in the spherical phase and near to the surface of a second order phase transition.

APPENDIX

In section IV the geometrical mapping of the Hamiltonian was shortly reviewed. As a trial state the coherent state, as defined in (22), was used. For a static problem, considered here, the variables (α_m, m= -1, 0, +1) of the coherent state satisfy the property under complex conjugation

$$\alpha^m = \alpha_m^* = (-1)^{1-m}\alpha_{-m}. \tag{25}$$

The scalar product of $\boldsymbol{\alpha}$ with itself is just

$$(\boldsymbol{\alpha}\cdot\boldsymbol{\alpha}) = \sum_m \alpha_m\alpha^m \;=\; \sum_m (-1)^{1-m}\alpha_m\alpha_{-m}, \tag{26}$$

which we denote by α^2. The α is the norm of the $\boldsymbol{\alpha}$, which can be related to the distance between the two clusters [21]. The potential is a pure function in α^2.

The scalar product of this variable with the π-boson creation operator or the π-boson annihilation operator are given by

$$\left(\boldsymbol{\alpha}\cdot\boldsymbol{\pi}^{\dagger}\right)=\sum_{m}\alpha^{m}\boldsymbol{\pi}_{m}^{\dagger},\qquad\left(\boldsymbol{\alpha}\cdot\boldsymbol{\pi}\right)=\sum_{m}\alpha_{m}\boldsymbol{\pi}^{m}. \tag{27}$$

In the geometrical mapping, expectation values of the operators with respect to the coherent state are calculated. A simple rule suffices in order to obtain the mapping:

$$\begin{aligned}\left\langle\boldsymbol{\alpha}\right|\boldsymbol{O}\left|\boldsymbol{\alpha}\right\rangle=\mathcal{N}_{N,n_0}^{2}\frac{N!^{2}}{(N+n_0)!^{2}}\frac{d^{n_0}}{d\gamma_1^{n_0}}\frac{d^{n_0}}{d\gamma_2^{n_0}}\\ \left\langle 0\right|\left[\boldsymbol{\sigma}+\gamma_1\left(\boldsymbol{\alpha}\cdot\boldsymbol{\pi}^{\dagger}\right)\right]^{N+n_0}\left|\boldsymbol{O}\right|\left[\boldsymbol{\sigma}+\gamma_2\left(\boldsymbol{\alpha}\cdot\boldsymbol{\pi}^{\dagger}\right)\right]^{N+n_0}\left|0\right\rangle,\end{aligned} \tag{28}$$

where after the differentiation one has to set γ_1 and γ_2 equal to 1.

There exists a simple rule for applying the operator, which is a function of the annihilation and creation operators, before differentiation, *i.e.* in the calculation of

$$\left\langle 0\right|\left[\boldsymbol{\sigma}+\gamma_1\left(\boldsymbol{\alpha}\cdot\boldsymbol{\pi}\right)\right]^{N+n_0}\left|\boldsymbol{O}\right|\left[\boldsymbol{\sigma}^{\dagger}+\gamma_2\left(\boldsymbol{\alpha}\cdot\boldsymbol{\pi}^{\dagger}\right)\right]^{N+n_0}\left|0\right\rangle.$$

First one has to pass all the creation operator to the left and all annihilation operators to the right. Then, one applies the annihilation operators one by one to the right and the creation operators one by one to the left. The results is a simple substitution

$$\begin{aligned}\boldsymbol{\pi}^{m}\left[\boldsymbol{\sigma}^{\dagger}+\gamma_2\left(\boldsymbol{\alpha}\cdot\boldsymbol{\pi}^{\dagger}\right)\right]^{N+n_0}\left|0\right\rangle&\rightarrow\left(N+n_0\right)\gamma_2\alpha^{m}\left[\boldsymbol{\sigma}^{\dagger}+\gamma_2\left(\boldsymbol{\alpha}\cdot\boldsymbol{\pi}^{\dagger}\right)\right]^{N+n_0-1}\left|0\right\rangle\\ \left\langle 0\right|\left[\boldsymbol{\sigma}+\gamma_1\left(\boldsymbol{\alpha}\cdot\boldsymbol{\pi}\right)\right]^{N+n_0}\boldsymbol{\pi}_{m}^{\dagger}&\rightarrow\left\langle 0\right|\left[\boldsymbol{\sigma}+\gamma_1\left(\boldsymbol{\alpha}\cdot\boldsymbol{\pi}\right)\right]^{N+n_0-1}\left(N+n_0\right)\gamma_1\alpha_{m}\\ \boldsymbol{\sigma}\left[\boldsymbol{\sigma}^{\dagger}+\gamma_2\left(\boldsymbol{\alpha}\cdot\boldsymbol{\pi}^{\dagger}\right)\right]^{N+n_0}\left|0\right\rangle&\rightarrow\left(N+n_0\right)\left[\boldsymbol{\sigma}+\gamma_2\left(\boldsymbol{\alpha}\cdot\boldsymbol{\pi}^{\dagger}\right)\right]^{N+n_0-1}\left|0\right\rangle\\ \left\langle 0\right|\left[\boldsymbol{\sigma}+\gamma_1\left(\boldsymbol{\alpha}\cdot\boldsymbol{\pi}\right)\right]^{N+n_0}\boldsymbol{\sigma}^{\dagger}&\rightarrow\left\langle 0\right|\left[\boldsymbol{\sigma}+\gamma_1\left(\boldsymbol{\alpha}\cdot\boldsymbol{\pi}\right)\right]^{N+n_0-1}\left(N+n_0\right).\end{aligned} \tag{29}$$

This is for the first application. For the second one the N changes to $N-1$, etc.

The norm of the coherent state is obtained choosing $\boldsymbol{O}=\mathbf{1}$ and afterwards applying the differentiations with respect to γ_1 and γ_2. The result contains a function $F_{00}(\alpha^2)$. When the operator contains powers in the π creation and annihilation

operators, the further function F_{pq} appear, which are of the form

$$F_{pq}\left(\alpha^2\right) = \frac{N!^2}{(N+n_0)!} \sum_{k=\max(n_0-p,n_0-q,0)}^{N+n_0-\max(p,q)} \left(\begin{array}{c} N+n_0-\max(p,q) \\ k \end{array} \right) \times \left[\frac{(k+p)!}{(k+p-n_0)!}\right] \left[\frac{(k+q)!}{(k+q-n_0)!}\right] \alpha^{2k} \quad (30)$$

Acknowledgments. Financial assistance from DGAPA-PAPIIT (No. IN103212) and CONACyT is gratefully acknowledged.

We also acknowledge very fruitful discussions with and comments of J. Cseh, J. Darai and G. Lévai.

REFERENCES

1. H. Yépez-Martínez, J. Cseh, P. O. Hess, Phys. Rev. **74**, 024319 (2006).
2. P. R. Fraser, H. Yépez-Martínez, , P. O. Hess, L. Parra-Rodríguez, J. Phys.: Conf. Ser. (2011).
3. H. Yépez-Martínez, P. R. Fraser, P. O. Hess, Phys. Rev. C **85**, 014316 (2012).
4. P. R. Fraser, H. Yépez-Martínez, P. O. Hess, Phys. Rev. C **85**, 014317 (2012).
5. J. Cseh, Phys. Lett. B **281**, 173 (1992).
6. J. Cseh, G. Lévai, Ann. Phys. (N.Y.) **230**, 165 (1994).
7. F. Iachello, Phys. Rev. C **23**, 2778 (1981).
8. J. P. Elliot, Proc. R. Soc. A **245**, 128; 562 (1958).
9. H. J. Daley, F. Iachello, Ann. Phys. (N.Y.) **167**, 73 (1986).
10. H. J. Daley, B. Barrett, Nucl. Phys. A **449**, 256 (1986).
11. K. Wildermuth, Y. C. Tang, *A Unified Theory of the Nucleus*, (Vieweg, Braunschweig1977).
12. A. Matic, A. M. van der Berg, M. N. Harakeh, W. Wörtsche, *et al.*, Phys. Rev. C **80**, 055804 (2009).
13. G. Lévai, J. Cseh, W. Scheid, Phys. Rev. C **46**, 548 (1992).
14. A. Sandulescu, D. N. Poenaru, W. Greiner, Sov. J. Part. Nucl. **11**, 528 (1980).
15. J. Cseh, J. Phys.: Conf. Ser. **205**, 012021 (2010).
16. H. Yépez-Martínez, L. Parra-Rodríguez, P. O. Hess, J. Cseh, G. Lévai, J. Phys.: Conf. Ser. **239**, 012005 (2010).
17. O. Castaños, P. O. Hess, P. Rochford, J. P. Draayer, Nucl. Phys. A **524**, 469 (1991).
18. R. B. Firestone, *et al.*, *Table of Isotopes*, (John Wiley & Sons, New York1996), 8th edn.
19. D. R. Tilley, H. R. Weller, C. M. Cheves, R. M. Chasteler, Nucl. Phys. A **595**, 1 (1995).
20. R. B. Firestone, Nucl. Data Sheets **108**, 2319 (2007).
21. P. O. Hess, G. Lévai, J. Cseh, Phys. Rev. C **54**, 2345 (1996).
22. J. Escher, J. P. Draayer, J. Math. Phys **39**, 5123 (1998).
23. J. Cseh, G. Lévai, P. O. Hess, W. Scheid, Few-Body Systems **29**, 61 (2000).
24. Eisenberg, Greiner, *Nuclear Theory I: Nuclear Models*, (North-Holland, Amsterdam1988), 2nd edn.
25. J.Cseh, G. Lévai, K. Kato, Phys. Rev. C **43**, 165 (1991).
26. P. O. Hess, Ş. Mişicu, Phys. Lett. B **595**, 187 (2004).

27. R. Blendowske, T. Walliser, Phys. Rev. Lett. **61**, 1930 (1988).
28. P. O. Hess, P. Rosales, E. Aguilera, A. Algora, J. Cseh, J. P. Draayer, T. L. Belyaeva, AIP Conf. Proc. **802**, 69 (2005).
29. P. O. Hess, A. Algora, J. Cseh, J. P. Draayer, Phys. Rev. C **70**, 051303 (2004).
30. K. Katō, H. Band**o**, Prog. Theo. Phys. **59**, 774 (1978).
31. P. O. Hess, G. Lévai, J. Cseh, Phys. Rev. C **54**, 2345 (1996).
32. D. J. Rowe, Rep. Prog. Phys. **48**, 1419 (1985).
33. O. Castaños, J. P. Draayer, Y. Leschber, Z. F. Phys. A **329**, 33 (1988).
34. M. Yasue, T. Hasegawa, S. I. Hayakawa, *et al.*, Phys. Rev. C **46**, 1242 (1992).
35. P. Cejnar, J. Jolie, Prog. in Part. and Nucl. Phys. **62**, 210 (2009).